AFRL-VS-HA-TR-2004-1008
E.R.P., No. 1253

NPOESS Scintillation Study

Bamandas Basu

6 Oct 2003

AIR FORCE RESEARCH LABORATORY
Space Vehicles Directorate
29 Randolph Rd
AIR FORCE MATERIEL COMMAND
Hanscom AFB, MA 01731-3010

This technical report has been reviewed and is approved for publication.

/ signed /
John B. Wissler, LtCol, USAF, Director
Battlespace Environment Division

/ signed /
Bamandas Basu
Author

/ signed /
Robert A. Morris, Chief
Space Weather Center of Excellence

This report has been reviewed by the AFRL/VS Public Affairs Office (PA) and is releasable to the National Technical Information Service (NTIS).

Qualified requestors may obtain additional copies from the Defense Technical Information Center (DTIC). All others should apply to the National Technical Information Service.

If your address has changed, if you wish to be removed from the mailing list, or if the addressee is no longer employed by your organization, please notify AFRL/VSIM, 29 Randolph Rd., Hanscom AFB, MA 01731-3010. This will assist us in maintaining a current mailing list.

Do not return copies of this report unless contractual obligations or notices on a specific document require that it be returned.

REPORT DOCUMENTATION PAGE

Form Approved
OMB No. 0704-0188

1. REPORT DATE *(DD-MM-YYYY)*	2. REPORT TYPE	3. DATES COVERED *(From - To)*
6 October 2003	Scientific, Final	May 2002-Sep 2003

4. TITLE AND SUBTITLE
NPOESS Scintillation Study

5a. CONTRACT NUMBER

5b. GRANT NUMBER

5c. PROGRAM ELEMENT NUMBER

6. AUTHOR(S)
Bamandas Basu

5d. PROJECT NUMBER
SMC0

5e. TASK NUMBER
SD

5f. WORK UNIT NUMBER
42

7. PERFORMING ORGANIZATION NAME(S) AND ADDRESS(ES)
Air Force Research Laboratory/VSBXP
29 Randolph Road
Hanscom AFB, MA 01731-3010

8. PERFORMING ORGANIZATION REPORT NUMBER
AFRL-VS-HA-TR-2004-1008

9. SPONSORING/MONITORING AGENCY NAME(S) AND ADDRESS(ES)
Space and Missiles Center

Los Angeles, CA

10. SPONSOR/MONITOR'S ACRONYM(S)

11. SPONSOR/MONITOR'S REPORT NUMBER(S)

12. DISTRIBUTION/AVAILABILITY STATEMENT
Approved for public release; distribution unlimited

13. SUPPLEMENTARY NOTES

14. ABSTRACT

Theoretical study of the total electron content (TEC) in the nighttime equatorial anomaly region shows that linear relationships with statistically significant correlation coefficients exist between the maximum value of the post-sunset enhanced plasma drift velocity and the peak-to-valley ration of anomaly TEC. The maximum value of the post-sunset vertical plasma drift velocity is an important, perhaps the most important, parameter for determining both the intensity and the latitudinal distribution of equatorial scintillation. When this parameter is not available from any direct measurement, the relationships may be used to estimate it from the peak-to-valley ratio of anomaly TEC, which, in turn, can be derived from the ultraviolet (UV) imagery data of the anomaly region acquired by NPOESS sensors and NPOESS-heritage sensors; e.g. GUVI on TIMED and SSUSI on DMSP. This indicates the possibility of NPOESS data being used for a scintillation-forecasting scheme. The relationships presented here are valid for the longitude sector of the Jicamarca incoherent scatter radar whose drift velocity measurements have been used in the ambient plasma density model for TEC calculations. Similar relationships for other longitudinal sectors need to be investigated.

15. SUBJECT TERMS
Equatorial anomaly Drift velocity TEC Scintillation UV measurements GUVI NPOESS

16. SECURITY CLASSIFICATION OF:			17. LIMITATION OF ABSTRACT	18. NUMBER OF PAGES	19a. NAME OF RESPONSIBLE PERSON
a. REPORT	b. ABSTRACT	c. THIS PAGE			Bamandas Basu
UNCL	UNCL	UNCL	UNL		19b. TELEPHONE NUMBER *(Include area code)* 781 377-3048

Table of Contents

List of Illustrations

Acknowledgements

The author expresses his sincere appreciation to K. Scro (SMC Det 11/WXT) and W. Denig (AFRL), who helped him in many ways, starting with the preparation of the research proposal. Appreciation is extended to my colleagues, J. M. Retterer and Odile de La Beaujardiere, for helpful conversations during the course of this work. Thanks are also due to C. Valladares (Boston College) for the GPS data and to my colleague D. T. Decker for the TOPEX data. The Jicamarca drift data were taken from the CEDAR Database. This work was supported by a NPOESS IPO grant (SMC0SD28).

1. Introduction

Scintillation caused by density fluctuations (irregularities) in the ionosphere results in outages of the communication and navigation systems that depend on trans-ionospheric radio links. The outages can be particularly severe at low magnetic latitudes in the post-sunset hours, when scintillation is caused by the occurrence of so-called plasma 'bubbles' (density depleted regions) that are formed as a result of the generalized Rayleigh-Taylor instability. Requirements for forecasting ionospheric scintillation are stated in the *Air Force Space Command Aerospace Weather Information Requirements* document, dated 02 April 2002. The required lead-time for scintillation forecasting varies from 1 hour to beyond 120 hours depending upon the individual unit and planning cycle supported. Current operational capabilities for scintillation forecasting are limited to climatological assessments from WideBand ionospheric scintillation MODel (WBMOD) and persistence techniques (eastward drift and decay of observed scintillation structures) as used in the Operational Space Environment Network Display (OpSEND) Ultra High Frequency Scintillation Maps. These state-of-the-art operational maps provide only a current specification and a limited, two-hour, forecast of ionospheric scintillation.

The objective of the present task is to develop a scheme for forecasting scintillation in the post-sunset equatorial ionosphere using NPOESS or NPOESS-like data. The plan is to accomplish the task in two phases. This report deals with the recently completed phase 1 of the task.

The peak value of the $\mathbf{E} \times \mathbf{B}$ vertical plasma drift velocity due to the post-sunset, enhanced eastward electric field $\mathbf{E}$ is now recognized as the most important parameter for determining both the intensity and the latitudinal distribution of equatorial scintillation

[*Fejer et al.*, 1999; *Whalen*, 2001]. Estimation of the peak value of the $\mathbf{E} \times \mathbf{B}$ vertical plasma drift velocity is therefore critical to any scintillation-forecasting scheme. In our proposed scheme, the peak value of the vertical plasma drift velocity will be estimated from measurements of the Appleton anomaly parameters, such as the magnitude of the anomaly crest and its latitudinal width, peak-to-valley ratio of the anomaly Total Electron Content (TEC), etc. It will then be used to drive the Air Force Research Laboratory (AFRL) model [*Retterer,* 1999; *Retterer et al.*, 2002] for simulation of plasma 'bubble' formation and calculation of amplitude scintillation index (S_4), leveraging the developmental work within the C/NOFS program. The scintillation-forecasting scheme will thus be based on the knowledge of the parameters characterizing the anomaly. These parameters can be derived from the ultraviolet (UV) imagery data of the anomaly region acquired by NPOESS sensors and NPOESS-heritage sensors; e.g. GUVI on TIMED and SSUSI on DMSP. Hence, NPOESS and NPOESS-like data will, in principle, be capable of being used to forecast the occurrence of scintillation and the magnitude of the amplitude scintillation index S_4.

As a first step towards developing the scintillation-forecasting scheme, a theoretical study was undertaken to derive and validate possible quantitative relationships between the peak value of the vertical plasma drift velocity and one or more of the various Appleton anomaly parameters. The relationship can then be used to estimate the peak value of the vertical plasma drift velocity from measurements of the anomaly parameter. The AFRL low-latitude ionosphere model [*Retterer,* 1999; *Retterer et al.*, 2002] was used for the study. The scientific rationale for the feasibility of such a scintillation-forecasting scheme is discussed in more detail in the following section.

2. Scientific Rationale

An interesting feature of the ionosphere at equatorial latitudes, which makes it quite different from that at other latitudes, is the so-called Appleton anomaly. During daytime, the eastward E-region dynamo electric field (**E**) from off-equatorial regions maps along the Earth's magnetic field (**B**) into F-region heights above the magnetic equator. The resulting $\mathbf{E} \times \mathbf{B}$ drift causes the F-region plasma to move vertically upward at the magnetic equator. The uplifted plasma then diffuses along **B** due to gravity and pressure gradient forces. This results in the formation of the Appleton anomaly with minimum F-region ionization density at the magnetic equator and maximum at the two crests at about ±14 to ±20 degrees magnetic latitude depending upon the peak value of the vertical plasma velocity. Near sunset, the E-region density and the E-region dynamo electric field decrease and the Appleton anomaly starts to diminish. However, after sunset when the E layer of the equatorial plasma virtually disappears due to rapid recombination of ions and electrons, the F-region dynamo, in the presence of the sunset induced conductivity gradient, regenerates the eastward electric field with significantly enhanced value. The vertical uplift of the plasma due to the F-region dynamo electric field and the subsequent diffusion process, as described above, result in the resurgence of the Appleton anomaly in the post-sunset period. At the same time, since the recombination rates decrease with increasing altitude, a sharp density gradient develops on the bottom side of the F layer, and the plasma on the bottom side of the F layer becomes unstable due to the combined effects of the gravity, the eastward electric field and the vertically downward neutral wind velocity (if there is any). The relevant plasma instability is known as the generalized Rayleigh-Taylor (GRT) instability. Subsequent nonlinear development of the

instability leads to the occurrence of 'bubbles', which cause scintillation. In the most elementary, yet quite informative, description of the GRT instability, the linear growth rate (γ) is given by [see e.g., *Kelley,* 1989; *Basu,* 1997, 1998, 2002]

$$\gamma = (g/\nu_{in} + V_E + V_N)/L_n \quad (1)$$

Here g is the acceleration due to gravity, ν_{in} is the ion-neutral collision frequency, V_E is the peak value of the vertically upward $\mathbf{E} \times \mathbf{B}$ velocity of the plasma, V_N is the vertically downward neutral wind velocity and L_n is scale length of the density gradient in the vertically upward direction. As is evident from Eq. (1), the peak value of the vertical plasma velocity V_E directly contributes to the linear growth rate. It also enhances the gravitational term (g/ν_{in}) in Eq. (1) by moving the plasma upward to higher altitudes where ν_{in} is smaller. Consequently, it plays an important role in the linear growth of the GRT instability and, hence, in the subsequent formation of 'bubbles' by nonlinear processes. Furthermore, scintillation is most disruptive [*Whalen,* 2000] when a 'bubble' encounters the maximum electron density of the Appleton anomaly, which, as described earlier, is also formed due to the vertical drift of the plasma, albeit by a different physical mechanism. The post-sunset vertical drift of the plasma does not attain sufficient magnitude on some days to cause the evening equatorial anomaly and the scintillation.

The preceding discussion attests to the fact that the peak value of the post-sunset vertical plasma velocity plays an important role both in the formation of the Appleton anomaly and in the occurrence of scintillation. Previous theoretical calculations of the ambient plasma density distribution in the nighttime equatorial ionosphere have shown that the structure of the Appleton anomaly indeed depends on the peak value of the post-sunset plasma drift velocity [*Anderson,* 1973]. In addition, recent analysis based on a

limited set of data from an array of ionospheric sounders indicated that the maximum density of the anomaly crest and the latitudinal width of the anomaly have linear dependence on the peak value of the vertical plasma drift velocity [*Whalen*, 2001].

3. Technical Approach

The technical approach for phase 1 is to calculate the electron density distributions as a function of altitude and latitude at a specific longitude and time, using the AFRL theoretical model of the low-latitude ambient ionosphere. The model uses the following input parameters as a function of location, time, solar activity, and geomagnetic activity:

1. The neutral densities and the neutral temperature are obtained from the MSIS model of *Hedin* [1986].
2. The horizontal components of the neutral wind velocity are obtained from the empirical wind model HWM of *Hedin et al.* [1991].
3. The electron and ion temperatures are based on the empirical model of *Brace and Theis* [1981].
4. Production and loss rates are calculated from the local model of *Jasperse* [1974]; production rates use the solar EUV fluxes derived from the algorithm of *Hinteregger et al.* [1981].
5. Zonal ion drifts are given by an empirical model [*Fejer et al.*, 1991] based on Jicamarca radar measurements. When vertical drift velocity information is not available, the model uses the empirical drift model [*Scherliess and Fejer*, 1999] based on measurements by the Jicamarca radar and the AE-E satellite.

Obviously, if real-time data for neutral densities, neutral wind velocity, electron and ion temperatures, and plasma drift velocities were available, the physics-based model would reproduce the low-latitude ambient ionosphere quite accurately. Unfortunately, that is not the case and we have to rely on models for these important input parameters. The adopted models for the input parameters do a fairly good job in reproducing the climatology; but, for the day-to-day variability of the parameters, improved models are desirable. The in-situ and ground-based measurements of neutral densities and neutral wind velocity, in coordination with the modeling efforts supplemental to the measurements, such as TIGCM, can provide the desired improvements. The C/NOFS mission is designed for such a purpose. In another area needing improvement, it is necessary to have either measurements or a physics-based model, instead of the current empirical model, for electron and ion temperatures, which determine both the recombination and the diffusion rates. The empirical model of *Scherliess and Fejer* {1999] for the vertical plasma drift velocity does a fairly good job in reproducing the climatology of the temporal behavior of the plasma drift velocity. But it often fails to predict the peak value of the post-sunset velocity accurately. A physics-based model is being developed at AFRL to calculate the enhanced eastward electric field after sunset. In the absence of drift data, this model, when combined with the empirical model, should yield a much better drift model. Alternatively, if the peak value of the drift velocity can be estimated from other measurements, as the present study suggests, that information may also be incorporated into the empirical model to make it more realistic.

In the present study, vertical plasma drift velocities measured by the Jicamarca incoherent-scatter radar (11.95° S, 283.13° E geographic, magnetic dip 2° N) are used in

the plasma density model. Specifically, F region average values of the drift velocity for fourteen days in 2002 (April 15 – 17, May 31 – June 1, June 3 – 4, October 8 – 10, and November 11 – 14), representing both equinox and solstice conditions, are used. These are the only days in 2002 for which the Jicamarca drift data are available. However, the peak values of the post-sunset drift velocity on these days range from about 10 m/s to about 70 m/s and so the data set is useful for the present study. Solar conditions were moderate for those days with the daily value of $F_{10.7}$ cm flux between 170 and 200 units, and the 3 hr average of daily Kp values ranges from 1.5 to 6.0.

One of the many outputs of the model is the latitudinal profile of the height-integrated electron density (TEC) at a specified longitude (longitude of Jicamarca radar in the present study) and at different times. For validation purpose, the latitudinal profiles given by the model are compared with those obtained from the GPS data and the dual frequency altimeter data from TOPography EXperiment (TOPEX), when available. The GPS data for TEC are obtained from a low-latitude chain of 10 receivers [*Valladares et al.*, 2001] that are located near the west coast of South America (~287° E longitude), which is close to the longitude of the Jicamarca radar, extending between 5° N and 37° S (geographic latitudes). From the latitudinal distribution of the calculated TEC, the various anomaly parameters such as the location and magnitude of the anomaly crest, the width of the anomaly, and the peak-to-valley ratio of anomaly TEC, etc. are determined. Repeating the calculations of TEC for the fourteen days in 2002, coefficients of correlation between the anomaly parameters and the peak value of the drift velocity are calculated and then theoretical relationships between them are determined by means of least squares fits.

4. Results

The four panels, (a) – (d), in Figure 1 show examples of the typical outputs of the AFRL ambient ionosphere model. Figure 1a shows the plasma drift velocity measured by the Jicamarca radar on 15 April 2002 as a function of universal time (UT) [~ 5 hours ahead of local time (LT)], which is used for obtaining the results presented in Figures 1b – 1d. It shows the daytime enhancement of the drift velocity near –0700 UT (~ 1200 LT) due to the E-region dynamo electric field and the post-sunset stronger enhancement near 0000 UT (~ 1900 LT) due to the F-region dynamo electric field, after which the drift velocity decreases and reverses its direction around 0100 UT (~ 2000 LT). Almost the same pattern is found for the drift velocity on all fourteen days. Figure 1b shows the calculated TEC at the magnetic latitude (MLAT) 16^{o} N and at the Jicamarca longitude as a function of local time. The magnetic latitude 16^{o} N has been chosen because the northern crests of both the daytime and the nighttime anomaly occur near it. The maximum TEC, near 1600 LT and 2100 LT, represents the daytime and nighttime anomalies, respectively. Figure 1c shows the latitudinal profiles of TEC at different selected times. It shows a weak (small peak-to-valley ratio of TEC) anomaly near sunset (1800 LT). After sunset, as the evening progresses, a well-defined anomaly begins to develop, and the TEC at the anomaly crests attains its maximum value around 2100 LT (shown in solid line) with the locations of the anomaly crests at about $\pm$ 16^{o} magnetic latitude. At later times, the TEC at the anomaly crests decreases, the locations of the anomaly crests move toward the magnetic equator, and eventually in the morning hours the anomaly disappears. This temporal behavior of the anomaly is in good agreement with that observed experimentally. Finally, Figure 1d shows the color-coded map of TEC

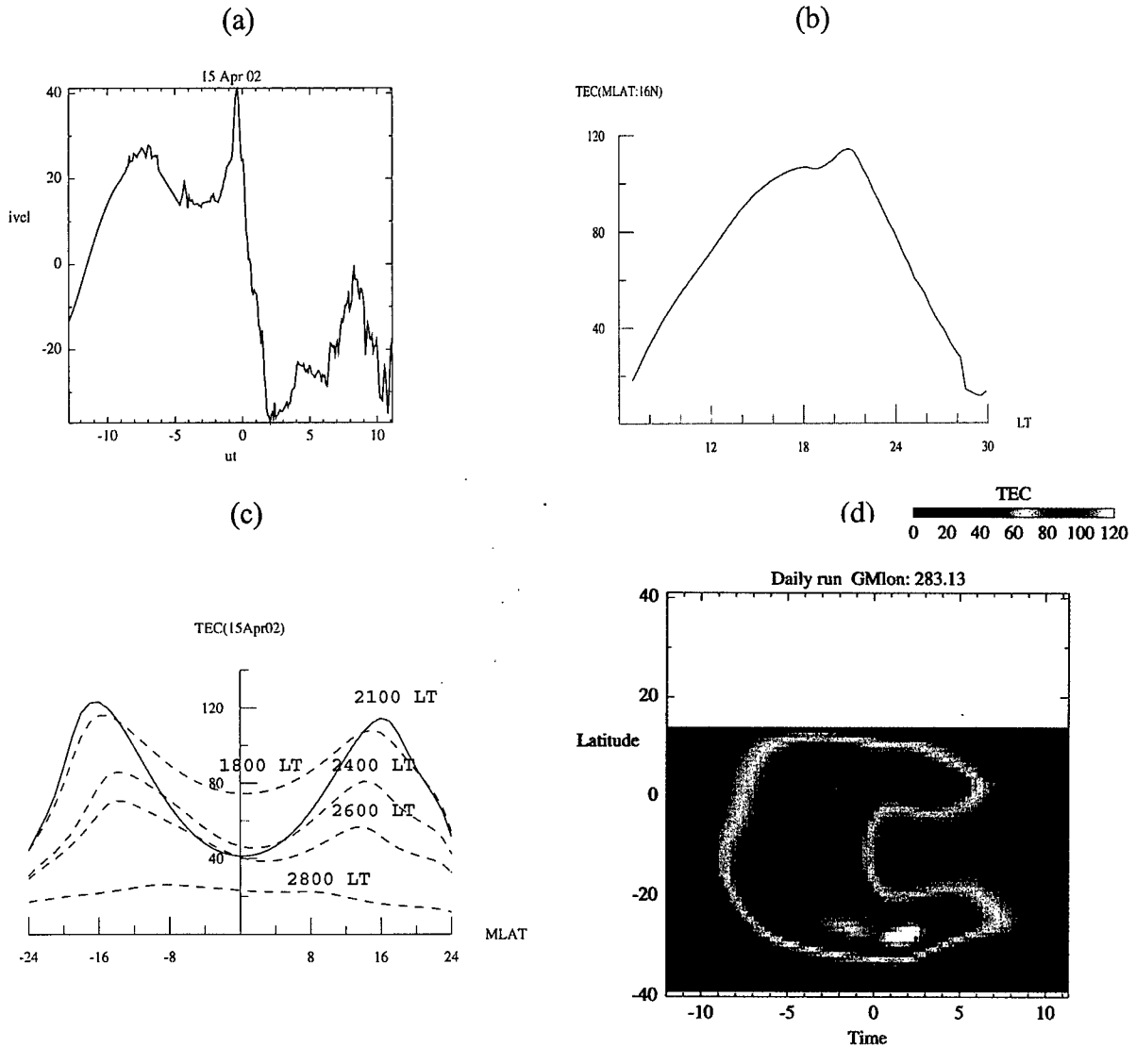

Figure 1. Example of the outputs of the AFRL ambient ionosphere model. (a) Drift velocity measured by Jicamarca radar on 15 April 2002 as a function of universal time (UT). (b) Model calculated TEC at the magnetic latitude (MLAT) 16° N and at the Jicamarca longitude as a function of local time. (c) Latitudinal profiles of calculated TEC at different selected times. (d) Color-coded map of TEC as a function of geographic latitude and universal time.

as a function of geographic latitude and universal time obtained for the drift data of April 15. It clearly shows the two anomaly crests and the temporal variation of their magnitudes, as well as the TEC minimum near the magnetic equator.

Figures 2 – 5 show comparisons between the latitudinal profiles of calculated TEC and those obtained from GPS measurements. The chosen examples represent different months in 2002. The four panels, (a) – (d), in each figure are for four different times indicated therein. The solid curve in each panel represents GPS data and the dashed curve represents model results. The dots in panel (c) of Figure 3 and panel (b) of Figure 4 represent TOPEX data. Considering the fact that real-time data has been used for just one of the several input parameters of the model, the agreements between model results and observations can be considered to be reasonably good.

The correlation between the peak value of the post-sunset drift velocity and the various anomaly parameters, such as the location and magnitude of the anomaly crest, the latitudinal width of the anomaly, and the peak-to-valley ratio of TEC at the anomaly, obtained from the theoretical model, have been studied. It is found that significant correlation exists only between the peak value of the post-sunset drift velocity and the peak-to-valley ratio of anomaly TEC. The six panels, (a) – (f), in Figure 6 show the scatter plots of the peak-to-valley ratio of model calculated TEC in the northern anomaly vs. maximum drift velocity (VM) for six selected times indicated therein. The straight line in each panel is the least squares fit to the scatter plot. The slope and intercept of the straight line as well as the value of the correlation coefficient (R) are indicated in each panel. At 0000 UT (~ 1900 LT), which is about the time when vertical plasma velocity on each day reaches its maximum value, the peak-to-valley ratios are almost independent of

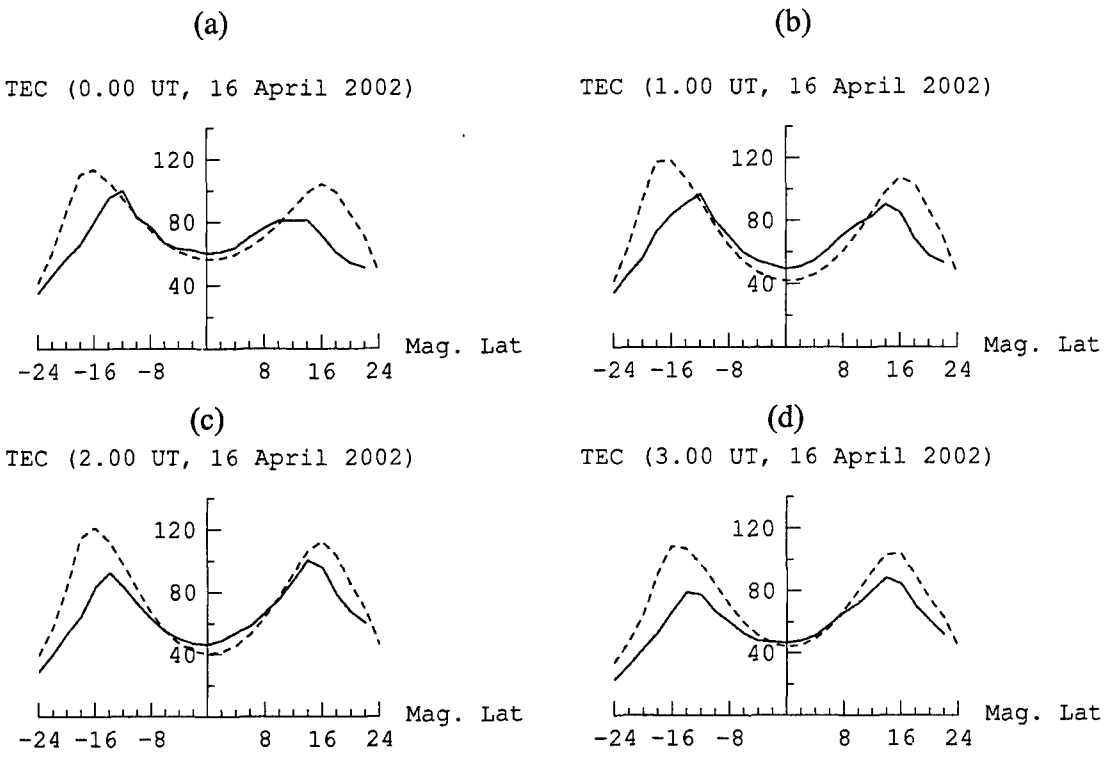

Figure 2. TEC on April 16, 2002 vs. magnetic latitude at four selected times: (a) 0000 UT; (b) 0100 UT; (c) 0200 UT; (d) 0300 UT. The dashed curves represent model results and the solid curves represent GPS data.

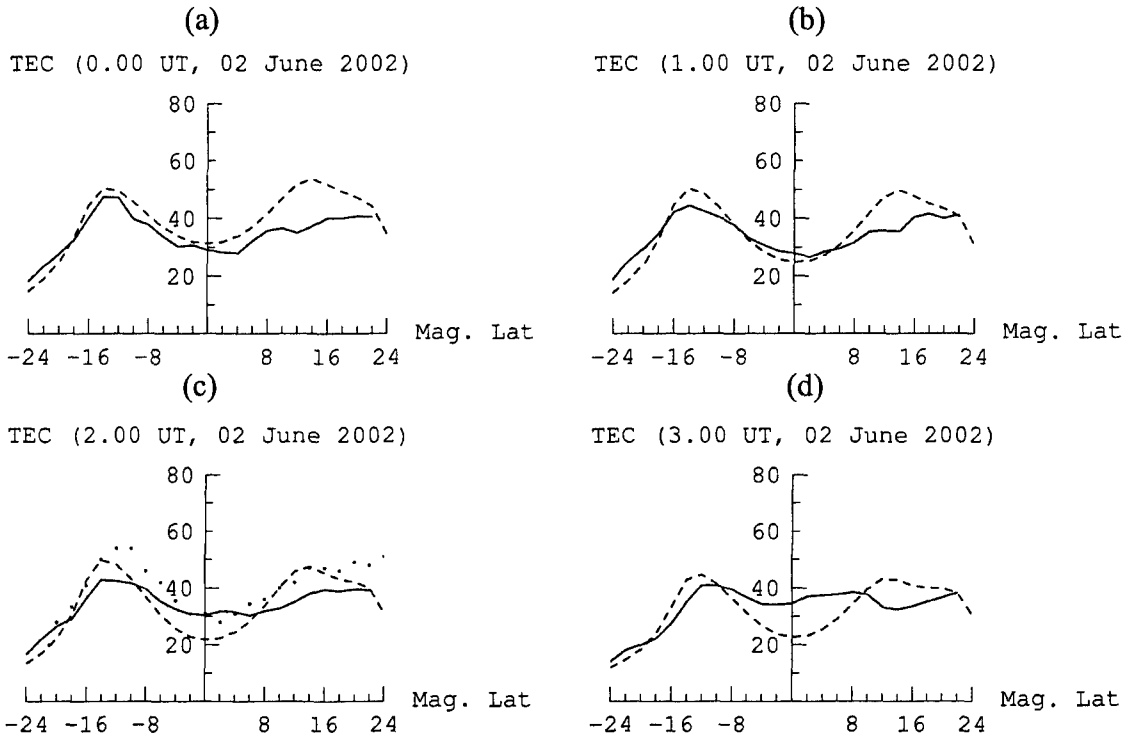

Figure 3. Same as in Figure 2, but for June 2, 2002. The dots in panel (c) represent TOPEX data.

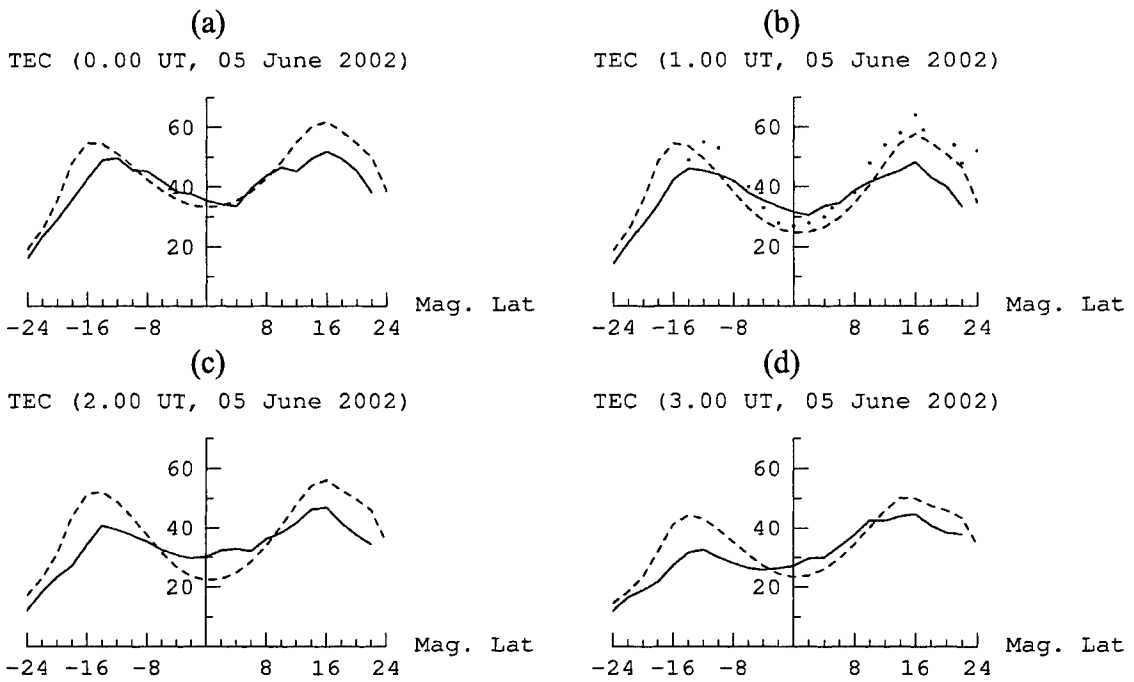

Figure 4. Same as in Figure 2, but for June 5, 2002. The dots in panel (b) represent TOPEX data.

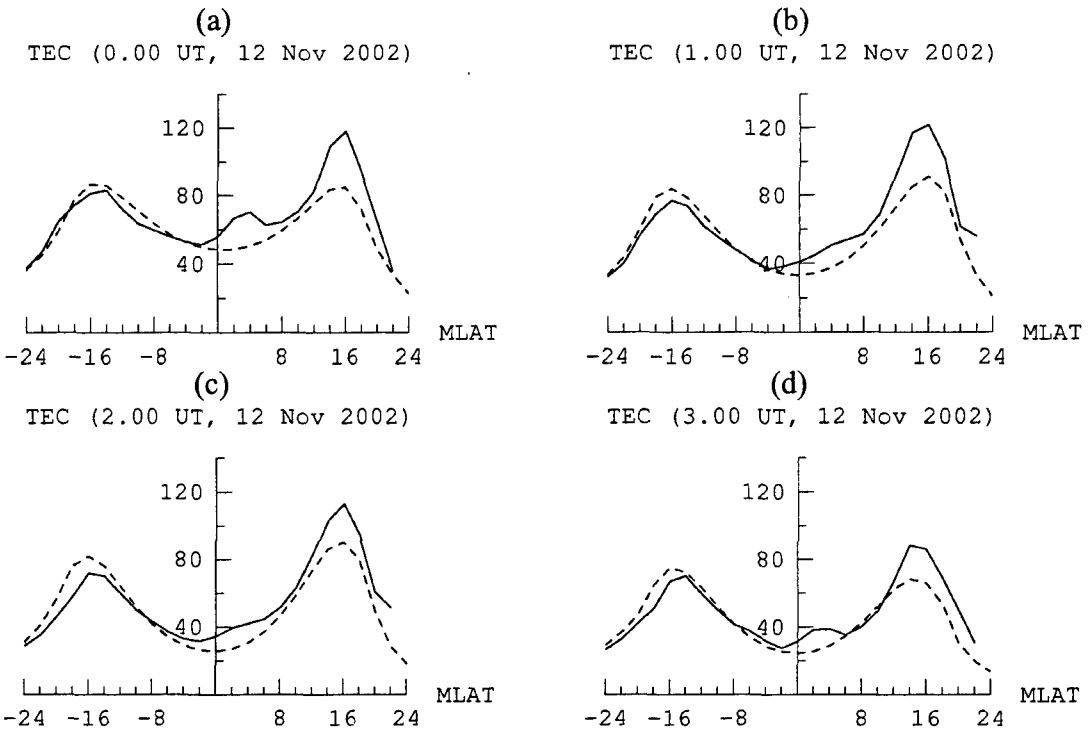

Figure 5. Same as in Figure 2, but for November 12, 2002.

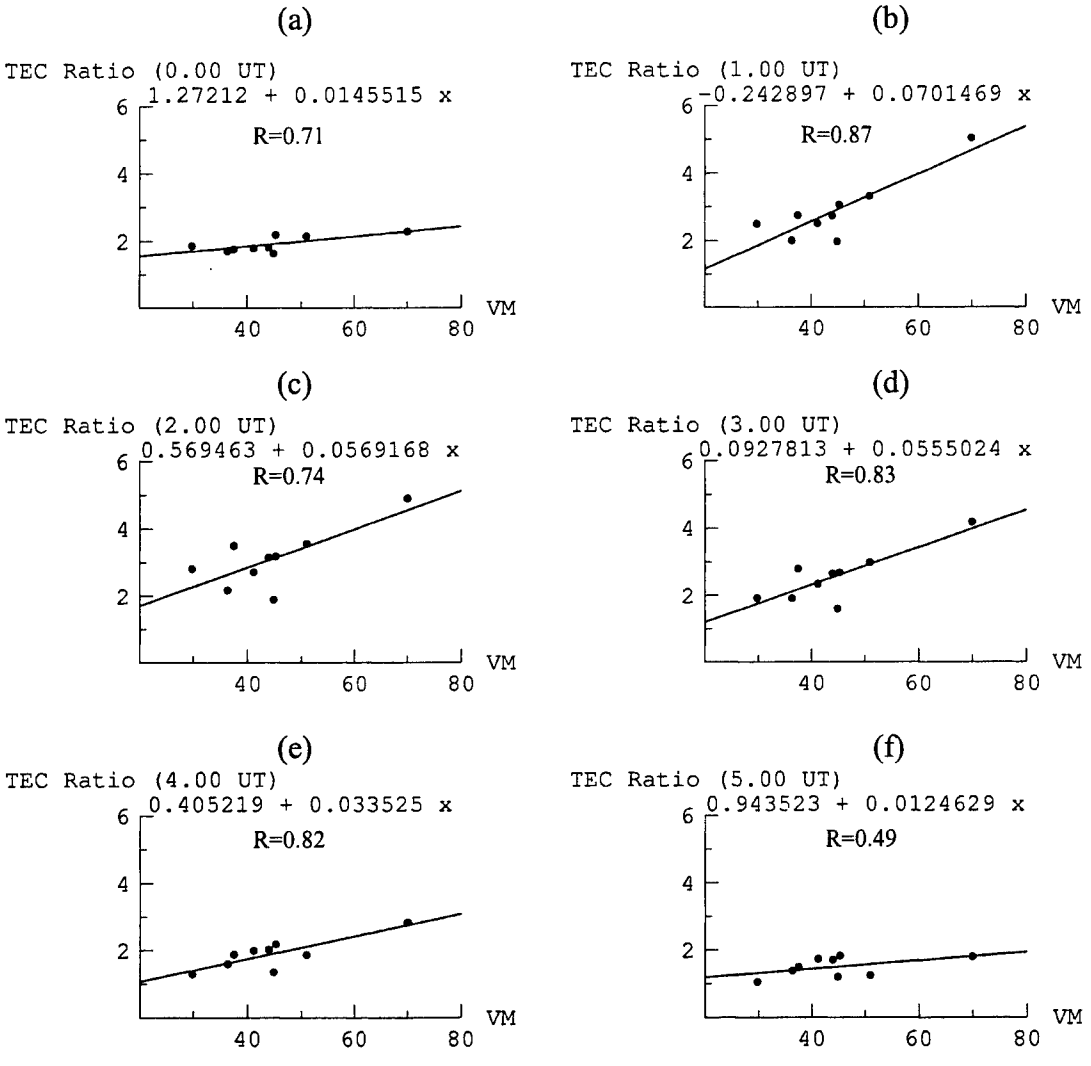

Figure 6. Scatter plots of the peak-to-valley ratio of model calculated TEC in the northern anomaly vs. maximum drift velocity (VM) for six selected times: (a) 0000 UT; (b) 0100 UT; (c) 0200 UT; (d) 0300 UT; (e) 0400 UT; (f) 0500 UT. The straight line in each panel is the least squares fit to the scatter plot. The slope and intercept of the straight line as well as the value of the correlation coefficient (R) are indicated in each panel.

the drift velocity. However, a definite linear dependence with a significant correlation coefficient becomes evident starting at 0100 UT (~ 2000 LT). This is physically explainable since it takes at least an hour for the ionosphere to 'feel' the effect of the post-sunset enhanced drift velocity. The linear dependence persists for about three hours. However, both the slope and the intercept of the regression line change with time. This is not surprising since the only constant feature of the Earth's ionosphere is its variability. The six panels, (a) – (f), in Figure 7 show the scatter plots of the peak-to-valley ratio of the model calculated TEC in the southern anomaly vs. maximum drift velocity (VM) for six selected times indicated therein. As in the case of the northern anomaly, a linear dependence is found starting at 0100 UT (~ 2000 LT) and seems to persist for a couple of hours. However, the correlation coefficients for the southern anomaly are evidently smaller than those found for the northern anomaly. The six panels, (a) – (f), in Figure 8 show the scatter plots of the location of the northern anomaly crest (LAC) in magnetic latitudes vs. the maximum drift velocity (VM) for the six selected times indicated therein. The straight line in each panel is the least squares fit to the scatter plot. The slope and intercept of the straight line as well as the value of the correlation coefficient (R) are indicated in each panel. The six panels (a) – (f), in Figure 9 show similar plots for the southern anomaly crest. Note that the correlation coefficients for the location of the anomaly crest are smaller than those for the peak-to-valley ratio of TEC. The coefficients of correlation for the other anomaly parameters are found to be even smaller. In Figures 6 – 9, results for the days when the peak value of the drift velocity is smaller than 30 m/s have been excluded. They are excluded because the empirical studies of *Fejer et al.* [1999] and *Whalen* [2001] indicate a threshold value of the peak vertical plasma velocity

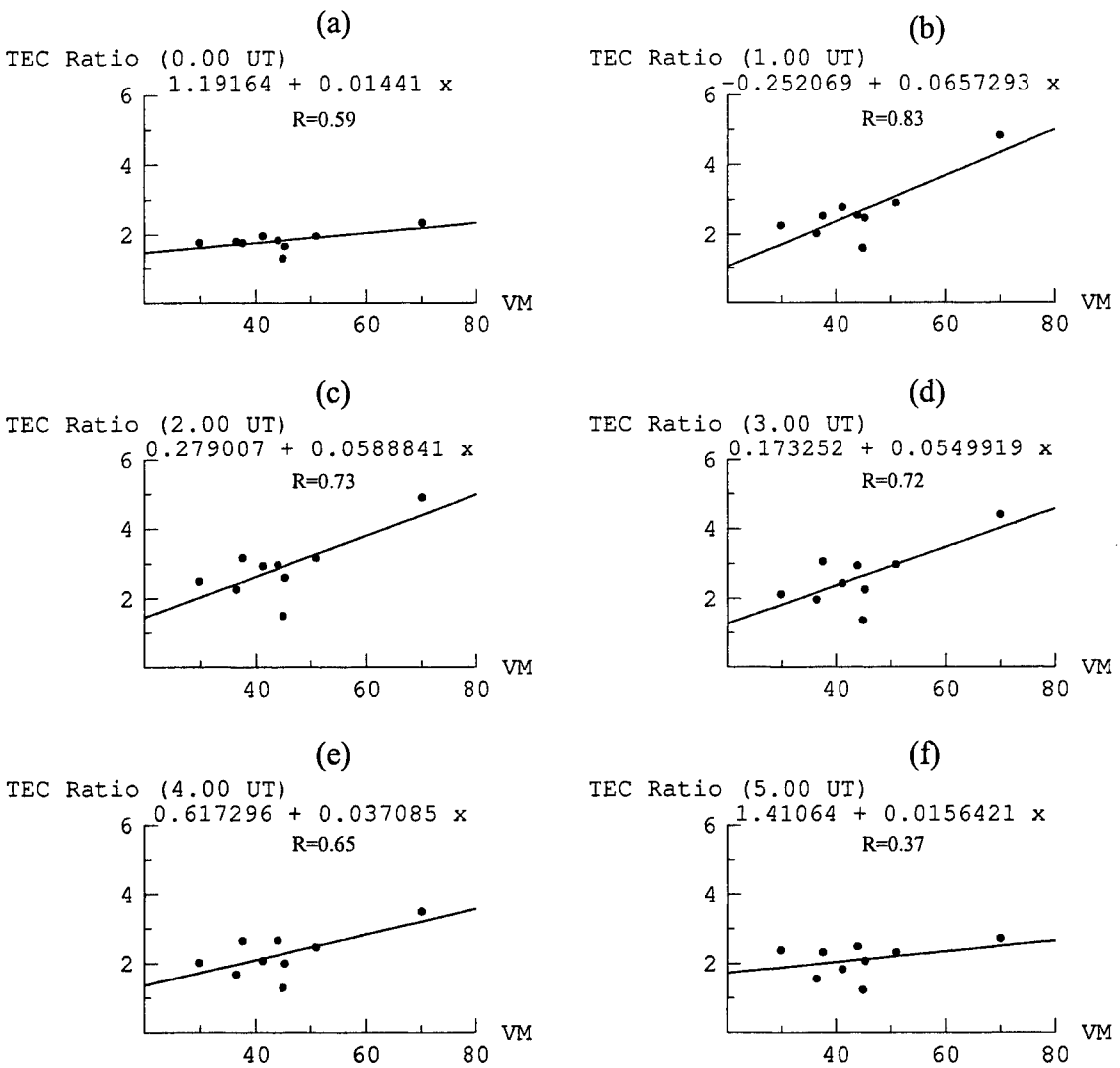

Figure 7. Same as in Figure 6, but for the southern anomaly.

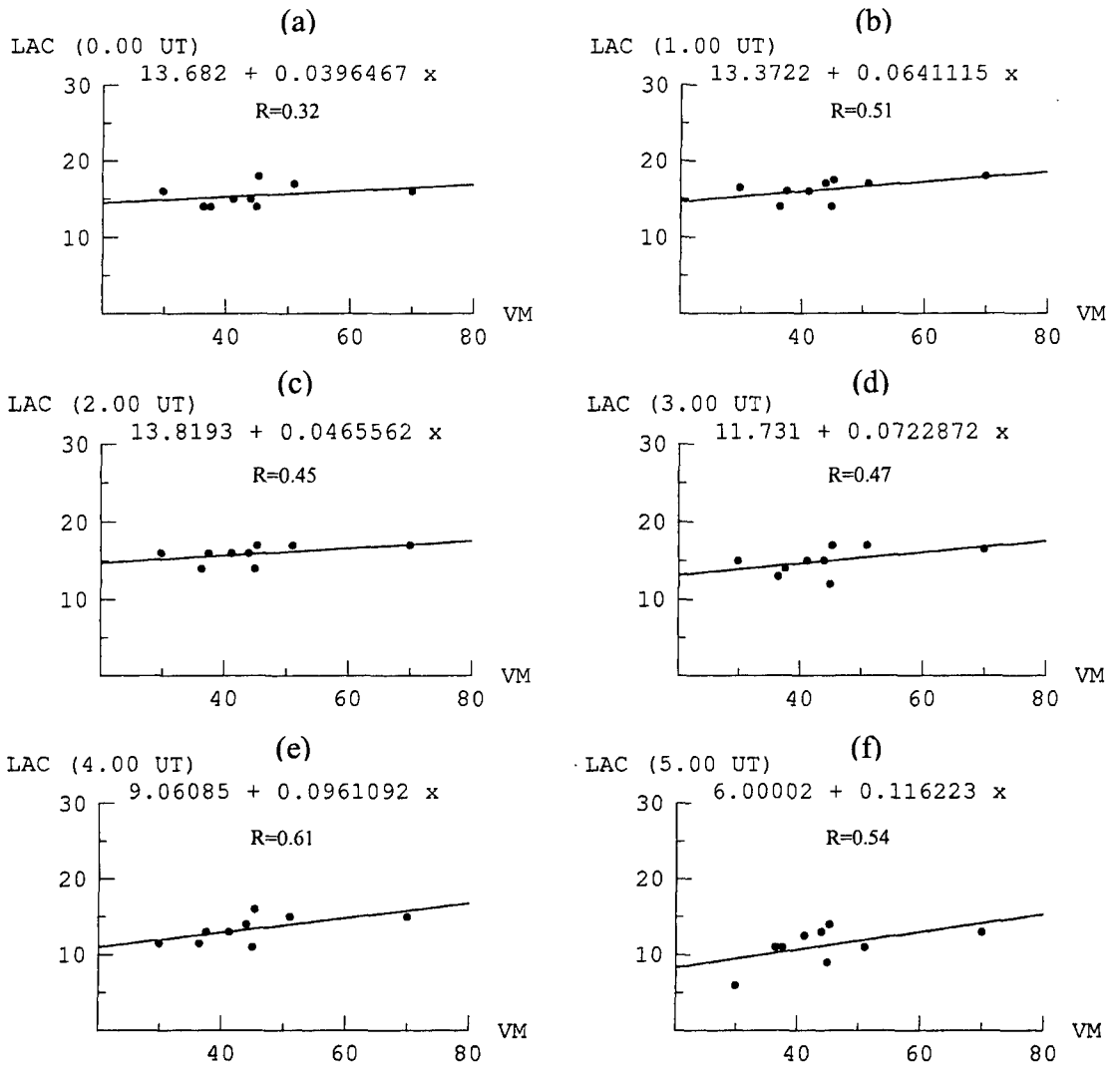

Figure 8. Scatter plots of the location of the northern anomaly crest (LAC) in magnetic latitudes vs. the maximum drift velocity (VM) for six selected times: (a) 0000 UT; (b) 0100 UT; (c) 0200 UT; (d) 0300 UT; (e) 0400 UT; (f) 0500 UT. The straight line in each panel is the least squares fit to the scatter plot. The slope and intercept of the straight line as well as the value of the correlation coefficient (R) are indicated in each panel.

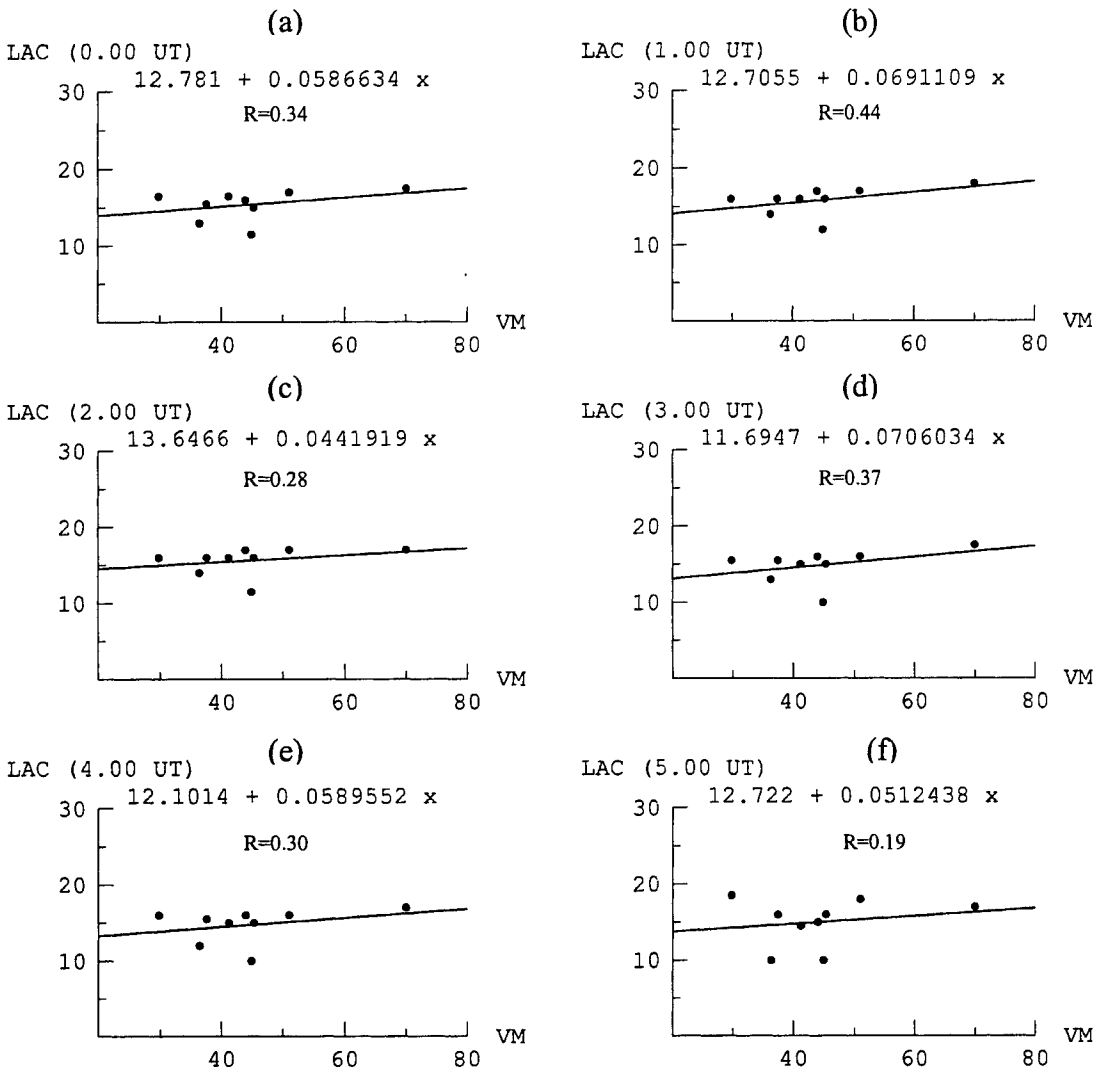

Figure 9. Same as in Figure 8, but for the southern anomaly crest.

for the scintillation to occur. This threshold value is 40 m/s.

The six panels, (a) – (f), in Figure 10 show the scatter plots of the peak-to-valley ratio of GPS measured TEC in the northern anomaly vs. maximum drift velocity (VM) for six selected times indicated therein. The straight line in each panel is the least squares fit to the scatter plot. The slope and intercept of the straight line as well as the value of the correlation coefficient (R) are indicated in each panel. The correlation coefficients are small at all times. The six panels, (a) – (f), in Figure 11 show the peak-to-valley ratios of GPS measured TEC in the southern anomaly vs. maximum drift velocity (VM) for six selected times indicated therein. The correlation coefficients (R) are small in this case too. If the somewhat stray data point corresponding to VM $\cong$ 51 m/s is excluded from Figure 11, the correlation coefficients at 0100 UT and 0200 UT become comparable to those obtained from the model results (see Fig. 7). This is shown in Figure 12. Similar improvements in the correlation coefficients are not obtained if we exclude the data point corresponding to VM $\cong$ 51 m/s from Figure 10.

5. Discussion

Theoretical study of the nighttime equatorial anomaly, based on the low-latitude ambient plasma density model at AFRL, shows that linear relationships, with significant correlation coefficients, exist between the peak value of the post-sunset enhanced plasma drift velocity and the peak-to-valley ratio of TEC in both the northern and the southern anomaly. The relationships are valid for the longitudinal sector of the Jicamarca incoherent scatter radar whose drift velocity measurements have been used in the model. Comparisons of model results with available data show reasonably good agreements on certain days, but not on other days. The theoretical calculations use real-time data for

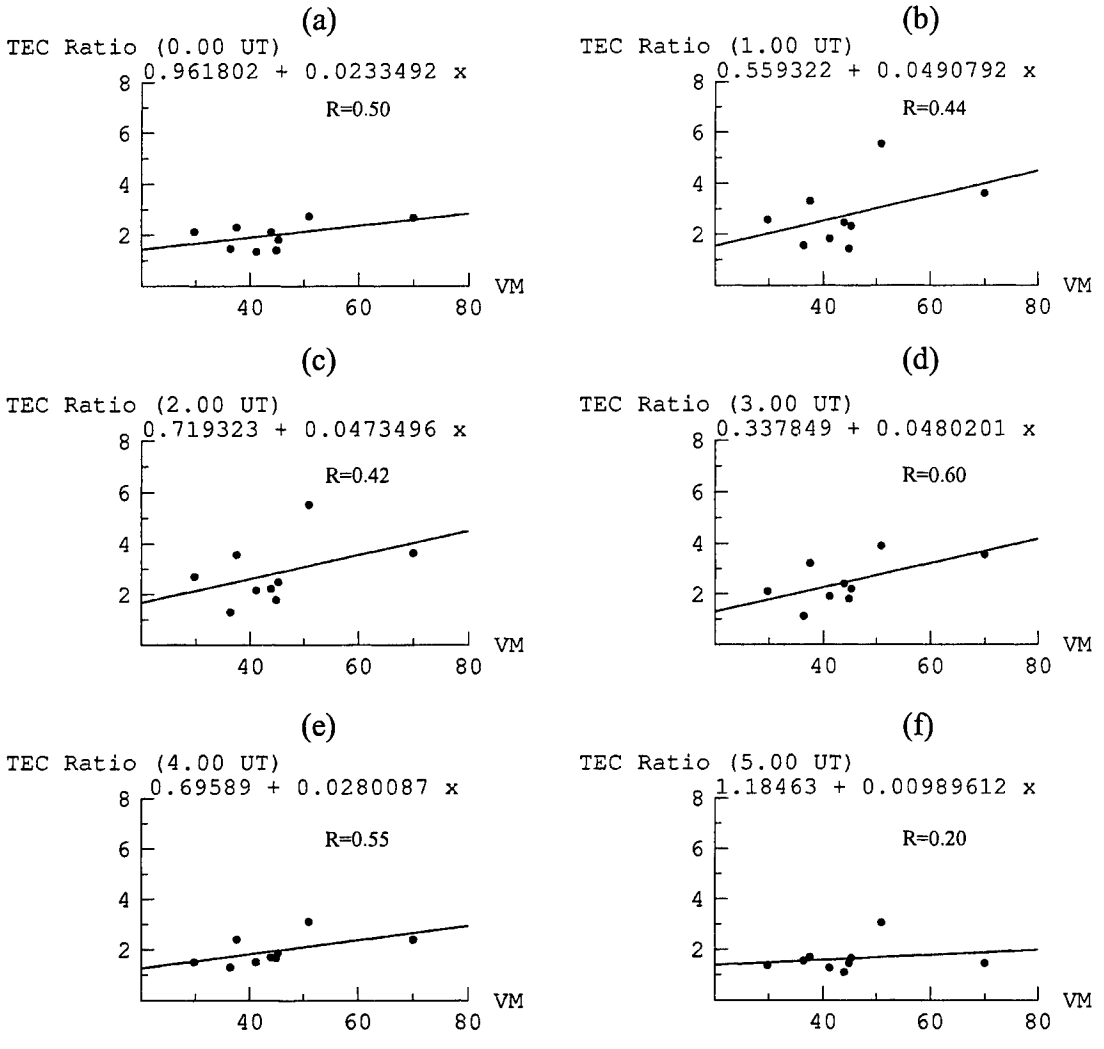

Figure 10. Scatter plots of the peak-to-valley ratio of GPS measured TEC in the northern anomaly vs. maximum drift velocity (VM) for six selected times: (a) 0000 UT; (b) 0100 UT; (c) 0200 UT; (d) 0300 UT; (e) 0400 UT; (f) 0500 UT. The straight line in each panel is the least squares fit to the scatter plot. The slope and intercept of the straight line as well as the value of the correlation coefficient (R) are indicated in each panel.

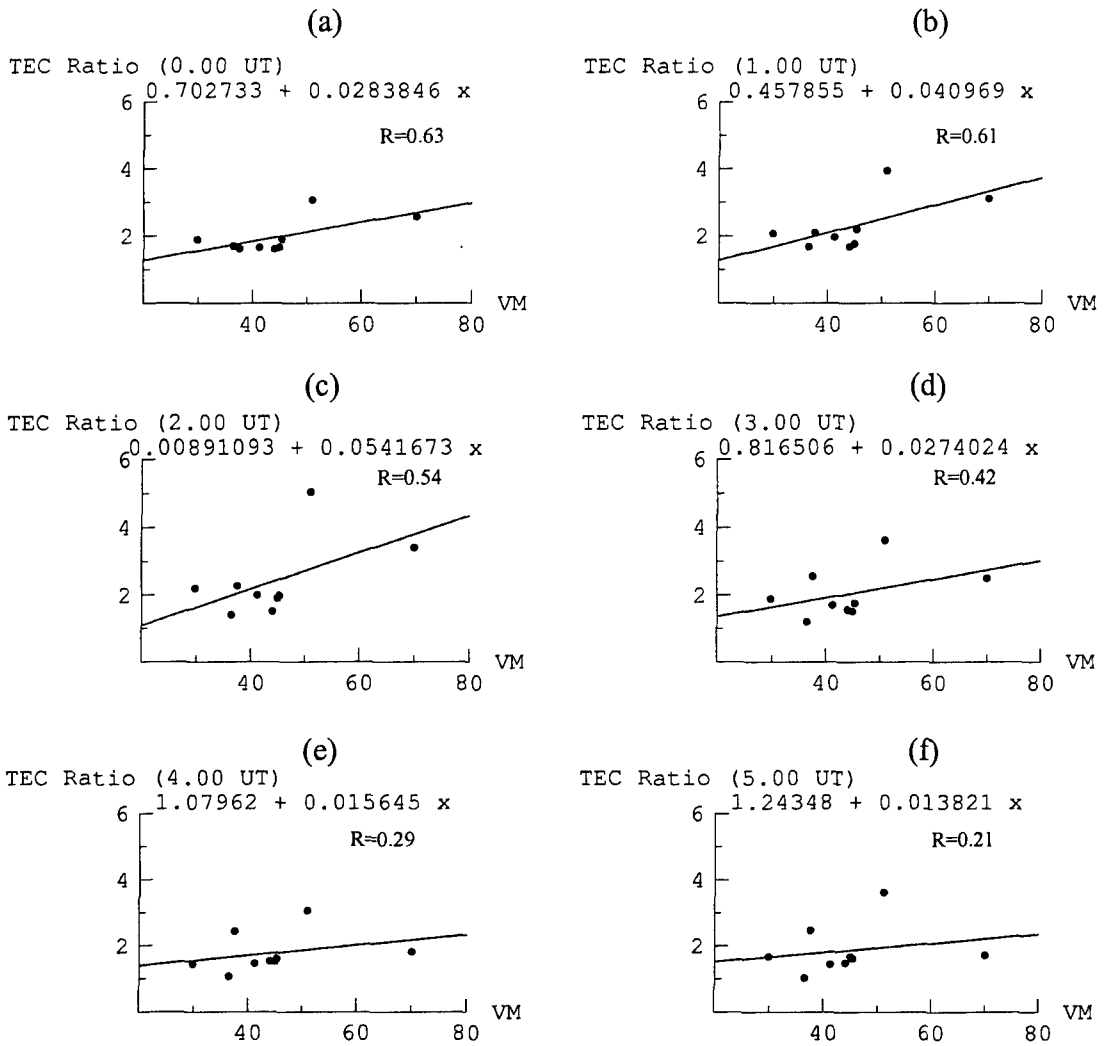

Figure 11. Same as in Figure 10, but for the southern anomaly.

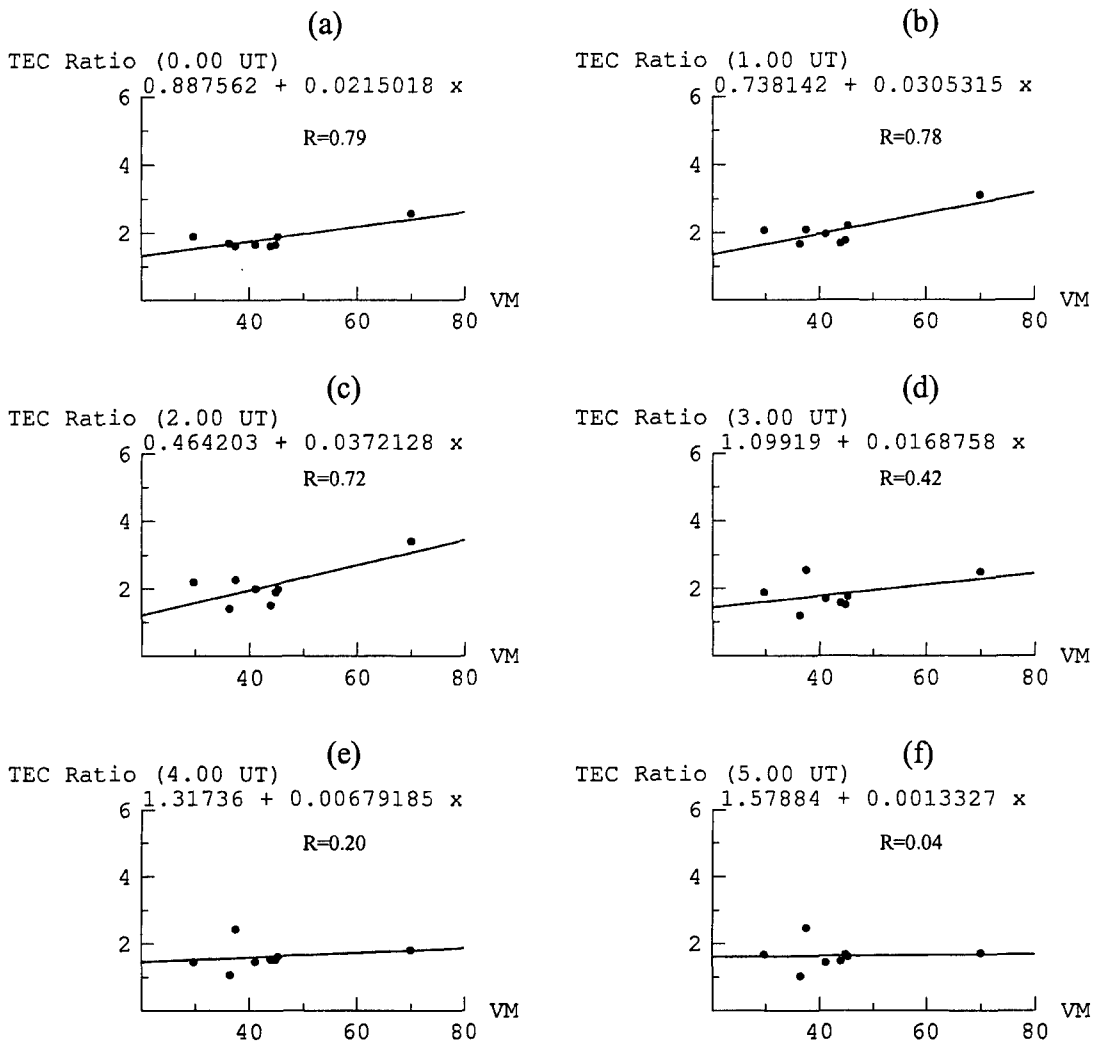

Figure 12. Same as in Figure 11 except that the data point corresponding to VM ≅ 51 m/s has been excluded. It shows improvement in the values of R at 0100 and 0200 UT.

only one input parameter, namely, the vertical plasma drift velocity. Empirical models specify other input parameters. Either real-time data or improved empirical models, such as those discussed earlier, for the input parameters need to be used in order to have more confidence in the theoretical model results.

The theoretical relations presented here may be used to estimate the peak value of the drift velocity from the measured value of the peak-to-valley ratio of anomaly TEC. The time dependence of the relations suggests that the relation that is appropriate at the time of measurement should be used. Such measurements are provided by GUVI on TIMED satellite, and will be provided by UV instruments on NPOESS satellite. In the absence of drift velocity data, the estimated peak value of the drift velocity may be incorporated into the empirical drift model of *Scherliess and Fejer* [1999] to make it more realistic. This drift model can then be used in the AFRL model for equatorial plasma bubble formation to forecast the occurrence of scintillation and the magnitude of the amplitude scintillation index S_4.

Two important issues have not been addressed. One important issue is the initial assessment of the improvement in the forecast of scintillation offered by this approach. The other important issue is whether or not similar relationships between the peak value of the drift velocity and the anomaly parameters exist in other longitudinal sectors. These issues should be addressed in phase 2.

After the work was completed, it came to our attention that *Bramley and Young* [1968] also investigated the effects of drift velocity on the formation and the structure of the equatorial Appleton anomaly and concluded that a linear relationship exists between the drift velocity and the peak-to-valley ratio of anomaly TEC. However, their

calculations and analyses were done for steady-state electron density distributions. The steady-state assumption is not a realistic assumption since the formation of the anomaly is a dynamic process with plasma loss and diffusion as well as the plasma drift velocity being time-dependent. The results of our calculations done with the time-dependent AFRL ionosphere model, assimilating drift velocity data, should be much more accurate.

References

Anderson, D. N. (1973) A theoretical study of the ionospheric F-region equatorial anomaly, I. Theory, *Planet. Space Sci.*, **21**, 409.

Basu, B. (1997) Generalized Rayleigh-Taylor instability in the presence of time-dependent equilibrium, *J. Geophys. Res.*, **102**, 17,305.

Basu, B. (1998) Equatorial plasma instability in time-dependent equilibrium, *Phys. Plasmas*, **5**, 2022.

Basu, B. (2002) On the linear theory of equatorial plasma instability: Comparison of different descriptions, *J. Geophys. Res.*, **107** (A8), 1199, doi: 10.1029/2001JA000317.

Bramley, E. N. and M. Young (1968) Winds and electromagnetic drifts in the equatorial F2 region, *J. Atmos. Terr. Phys.*, **30**, 99.

Fejer, B. G., E. R. de Paula, S. A. Gonzalez, and R. F. Woodman (1991) Average vertical and zonal F region plasma drifts over Jicamarca, *J. Geophys. Res.*, **96**, 13,901.

Fejer, B. G., L. Scherliess, and E. R. de Paula (1999) Effects of the vertical plasma drift velocity on the generation and evolution of equatorial spread F, *J. Geophys. Res.*, **104**, 19,859.

Hedin, A. E. (1987) MSIS-86 thermospheric model, *J. Geophys. Res.*, **92**, 4649.

Hedin, A. E. (1991) Revised global model of thermosphere winds using satellite and ground-based observations, *J. Geophys. Res.*, **96**, 7657.

Hinteregger, H. (1981) Observational, reference, and model data on solar EUV from measurements on AE-E, *Geophys. Res. Lett.*, **8**, 1147.

Jasperse, J. (1974) Electron distribution function and ion concentrations in the earth's lower ionosphere from Boltzmann-Fokker-Planck theory, *Planet. Space Sci.*, **25**, 743.

Retterer, J. M. (1999) Theoretical model for fast equatorial bubbles, in Proceedings of the 1999 *Ionospheric Effects Symposium*, J. M. Goodman (Ed.).

Retterer, J. M., D. T. Decker, W. S. Borer, R. E. Daniell, Jr., and B. G. Fejer (2003) Assimilative modeling of the equatorial ionosphere for scintillation forecasting: Modeling with vertical drifts, *J. Geophys. Res.*, submitted.

Scherliess, L. and B. G. Fejer (1999) Radar and satellite global equatorial F region vertical drift model, *J. Geophys. Res.*, **104**, 6829.

Valladares, C.E., S. Basu, K. Groves, M.P. Hagan, D. Hysell, A.J. Mazzella Jr., and R.E. Sheehan (2001) Measurement of the latitudinal distributions of total electron content during equatorial spread-F events, *J. Geophys. Res.*, **106**, 29,133.

Whalen, J. A. (2000) An equatorial bubble: Its evolution observed in relation to bottomside spread *F* and to the Appleton anomaly, *J. Geophys. Res.*, **105**, 5303.

Whalen, J. A. (2001) The equatorial anomaly: Its quantitative relation to equatorial bubbles, bottomside spread *F*, and $\mathbf{E} \times \mathbf{B}$ drift velocity during a month at solar maximum, *J. Geophys. Res.*, **106**, 29,125.